Cureus
Part of SPRINGER NATURE

Open Access Case Report

Intraperitoneal Small Round Cell Tumor Suggestive of Extraskeletal Ewing Sarcoma in an Eight-Year-Old Girl: Conversion to Resection and Adjuvant Volumetric Modulated Arc Therapy

Review began 10/15/2026
Review ended 10/26/2026
Published 10/30/2026

© **Copyright** 2026
Benhjar et al. This is an open access article distributed under the terms of the Creative Commons Attribution License CC-BY 4.0., which permits unrestricted use, distribution, and reproduction in any medium, provided the original author and source are credited.

DOI: 10.7759/cureus.118847

Fatima Benhjar [1], Soumiya Samba [1], Ahmed BenSghier [1], Soufiane Berhili [1], Mohamed Moukhlissi [1], Loubna Mezouar [1]

1. Department of Radiation Oncology, Faculty of Medicine and Pharmacy of Oujda, Mohammed First University, Mohammed VI University Hospital, Oujda, MAR

Corresponding author: Fatima Benhjar, benhjarf@gmail.com

Abstract

Intraperitoneal extraskeletal Ewing sarcoma (EES) is rare in young children and raises specific diagnostic and therapeutic challenges. An eight-year-old girl presented with fatigue, changes in bowel habits, and weight loss. Contrast-enhanced computed tomography (CT) revealed a large peritoneal and retroperitoneal mass (12.3 × 11 cm) encasing the major abdominal vessels, abutting the liver, with a separate small hepatic lesion. Core biopsy showed a small round cell tumor with diffuse CD99 positivity and negative staining for CD45, myogenin, desmin, chromogranin A, and synaptophysin, suggestive of EES. Testing for t(11;22) and EWSR1 rearrangement was unavailable and was not performed; the diagnosis was therefore considered probable EES pending molecular confirmation, and desmoplastic small round cell tumor (DSRCT) could not be excluded. After six cycles of VIDE (vincristine, ifosfamide, doxorubicin, and etoposide), CT showed a partial response, and the hepatic lesion had regressed. Because the mass remained unresectable, four cycles of VAI (vincristine, actinomycin D, and ifosfamide) were given before surgery. On preoperative CT, the primary mass measured 4.7 × 4.0 cm in the axial plane, a 62% decrease in its longest axial diameter. The resected specimen measured 6 × 4 × 3.5 cm and showed more than 90% treatment-related necrosis. The closest margin was less than 1 mm, and the resection was classified as microscopically incomplete (R1). Adjuvant volumetric modulated arc therapy was delivered; the planned boost was omitted, and the dose was limited to 45 Gy in 25 fractions to respect the dose constraints of adjacent organs. Treatment was completed with grade 1 acute gastrointestinal toxicity (nausea, diarrhea, and epigastric pain), and the patient had no evidence of recurrence at her last visit after a short follow-up.

This case illustrates the diagnostic uncertainty when molecular testing is unavailable and the balance between local control and the risks of abdominal irradiation in a child; longer follow-up is needed to assess treatment efficacy.

Categories: Radiation Oncology, Oncology, Pediatrics
Keywords: cd99, extraskeletal ewing sarcoma, intra-abdominal tumor, pediatric oncology, radiotherapy, small round cell tumor, vide chemotherapy

Introduction

Ewing sarcoma is the second most common primary malignant bone tumor in children and adolescents. It is an undifferentiated small round cell sarcoma characterized by a fusion involving the Ewing sarcoma breakpoint region 1 gene (EWSR1), or less commonly the fused in sarcoma gene (FUS), and an E26 transformation-specific (ETS) family transcription factor, most often Friend leukemia integration 1 (FLI1) [1,2]. Although usually associated with bone, Ewing sarcoma also arises in soft tissue. In a Surveillance, Epidemiology, and End Results (SEER) analysis of 2,202 patients, extraskeletal Ewing sarcoma (EES) accounted for 31% of cases and had a different clinical presentation from skeletal disease [3]. Registry and cooperative-group studies have reached different conclusions about the prognostic significance of an extraskeletal origin [4,5].

In children, EES most often affects the thorax and extremities; abdominal tumors are less common [6]. Reports of intestinal Ewing sarcoma illustrate the difficulties of diagnosing these tumors at visceral sites [7]. The differential diagnosis of an abdominal small round cell tumor includes desmoplastic small round cell tumor (DSRCT) [2,8]. When a tumor involves major vessels, surgery may be difficult, while radiotherapy is constrained by the nearby abdominal organs [1,9].

Intraperitoneal EES in young children is rare, and published experience consists mainly of isolated case reports, so management at this site is largely extrapolated from skeletal and extremity disease. We describe an eight-year-old girl with a large intraperitoneal tumor encasing the celiac trunk, superior mesenteric artery (SMA), and aorta, with a suspicious hepatic lesion on computed tomography (CT). A diagnosis of

How to cite this article
Benhjar F, Samba S, BenSghier A, et al. (October 30, 2026) Intraperitoneal Small Round Cell Tumor Suggestive of Extraskeletal Ewing Sarcoma in an Eight-Year-Old Girl: Conversion to Resection and Adjuvant Volumetric Modulated Arc Therapy. Cureus 18(10): e118847. DOI 10.7759/cureus.118847

probable EES, pending molecular confirmation, was made on morphological and immunohistochemical grounds, and DSRCT could not be excluded. This case illustrates three challenges: establishing the diagnosis when molecular testing is unavailable, achieving resection of an initially unresectable visceral tumor after prolonged induction chemotherapy, and delivering adjuvant radiotherapy after a microscopically incomplete resection when the surrounding abdominal organs limit the deliverable dose. We discuss the decisions that guided her treatment and the limitations of this approach.

Case Presentation

An eight-year-old girl was referred to our Pediatric Department for an abdominal mass. She reported anorexia, generalized fatigue, epigastric pain with vomiting, and alternating diarrhea and constipation, with a weight loss of 4 kg over two months. She was one of three children of non-consanguineous parents. Growth and development were normal, vaccinations were up to date, and there was no significant medical or surgical history. Her paternal grandfather had died of cancer of unknown type. She had initially been managed at a local hospital, where abdominal ultrasound showed only fecal stasis; further imaging was performed because her symptoms persisted. On examination, there was a solid, tender epigastric mass measuring approximately 9 × 8 cm, with hepatomegaly extending four finger-breadths below the costal margin and no splenomegaly. Vital signs and baseline laboratory values were not available in the records retrieved for this report.

Contrast-enhanced abdominopelvic CT performed at the referring hospital on Day 1 (initial diagnostic imaging) demonstrated a peritoneal and retroperitoneal mass measuring 11.4 × 9 cm in the axial plane and 11 cm craniocaudally. The mass encased the celiac trunk, the SMA, and the aorta, all of which were patent. It abutted the inferior and medial aspects of the liver with no clear tissue plane and displaced the patent portal vein. The stomach was shifted to the left. A staging CT of the brain, neck, chest, abdomen, and pelvis performed at our institution four days later (Day 5) showed the mass to measure 12.3 × 11.0 cm in the axial plane and 11.8 cm craniocaudally. There were also adjacent lymph nodes up to 10 × 9 mm, a rounded 13 × 11 mm enhancing lesion in segment III of the liver, and minimal ascites (Figure *1*).

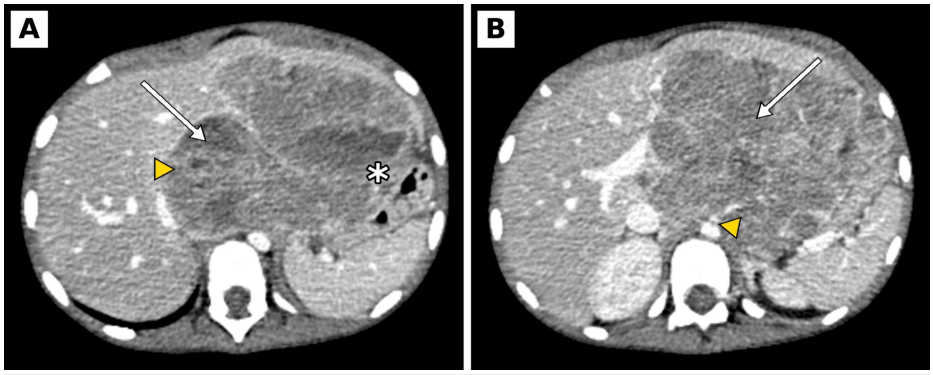


FIGURE 1: Baseline contrast-enhanced axial CT of the abdomen at two levels (A, upper; B, lower).

(A) The mass is in contact with the medial surface of the liver with no fat plane (yellow arrowhead) and displaces the stomach to the left (asterisk). (B) The mass extends posteriorly and encases the aorta, which is patent (yellow arrowhead).

A large heterogeneous, partly necrotic intraperitoneal mass is present in the upper abdomen (white arrows).

The staging CT described no distant lesion suspicious for malignancy apart from the hepatic lesion adjacent to the mass. Bilateral iliac crest bone marrow aspirates obtained on Day 8 were richly cellular and showed no non-hematopoietic cells. The referring radiologist suggested neuroblastoma or lymphoma. At our institution, the radiologist suggested a small round cell tumor and listed DSRCT, neuroblastoma, and peripheral primitive neuroectodermal tumor (PNET) as possible diagnoses; the differential diagnosis of such a tumor in this setting also includes lymphoma and rhabdomyosarcoma. The clinical presentation alone was non-specific and could not distinguish between these entities.

Ultrasound-guided core biopsy showed fibrous tissue infiltrated by small round cells with hyperchromatic nuclei and scant cytoplasm, with focal rosette formation. Immunohistochemistry demonstrated diffuse membranous cluster of differentiation 99 (CD99) staining and focal neuron-specific enolase (NSE) positivity. Staining for CD45 (leukocyte common antigen), myogenin, desmin, chromogranin A, and synaptophysin was negative (Figure *2*). The morphological and immunohistochemical findings were suggestive of a tumor within the Ewing sarcoma/PNET spectrum. The pathologist recommended testing for t(11;22) to confirm the diagnosis, but t(11;22) and EWSR1 rearrangement testing was unavailable at our hospital and was not

performed.

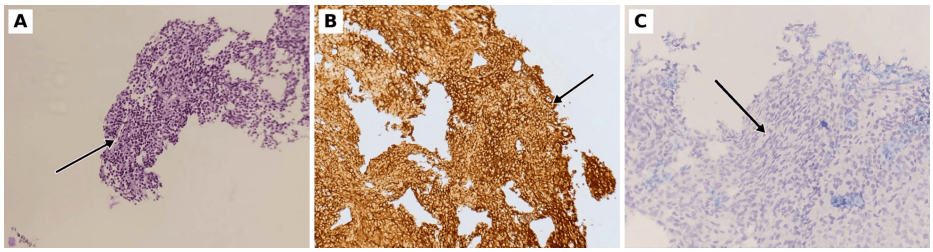


FIGURE 2: Histology of the ultrasound-guided biopsy of the abdominal mass.

(A) Hematoxylin and eosin (H&E) staining (original magnification ×100): diffuse proliferation of small round cells with hyperchromatic nuclei and scant cytoplasm (arrow). (B) Immunohistochemistry (original magnification ×200): diffuse membranous CD99 expression by tumor cells (arrow). (C) Immunohistochemistry (original magnification ×200): absence of staining of tumor cells (arrow) on a representative negative immunostain from the panel (CD45, myogenin, desmin, chromogranin A, and synaptophysin; hematoxylin counterstain).

Because molecular testing was not performed, the diagnosis in this patient should be regarded as probable EES pending molecular confirmation rather than definitive EES. It rests on morphology, a compatible immunohistochemical profile, and the subsequent response to Ewing-type chemotherapy; DSRCT, the main alternative diagnosis at this site, could not be formally excluded (see Discussion).

Chemotherapy followed the sequence of VIDE (vincristine, ifosfamide, doxorubicin, and etoposide) and VAI (vincristine, actinomycin D, and ifosfamide) used in the Euro-EWING99 program (Table *1*) [10]. The six VIDE cycles were administered from week 4 to month 4.5 after diagnosis, and the four VAI cycles from month 5 to month 8. Tumor response was assessed on contrast-enhanced CT according to Response Evaluation Criteria in Solid Tumors (RECIST) version 1.1 [11]. On the baseline CT (Day 5), the target lesions were the primary mass (longest axial diameter, 123 mm) and the segment III hepatic lesion (13 mm), giving a sum of longest diameters of 136 mm. The adjacent lymph node (10 × 9 mm) did not meet the RECIST size criterion for a target node (short axis of at least 15 mm) and was followed as a non-target lesion. Interim CT evaluations after three and six VIDE cycles were classified by the radiologist as partial responses, with regression of the hepatic lesion, which was not visualized on abdominal ultrasound after the fourth cycle. New findings after three cycles included mosaic attenuation in the lungs and cardiomegaly. After six VIDE cycles, the multidisciplinary tumor board still considered the mass unresectable, and two cycles of VAI were given. CT then showed stable disease, and two further VAI cycles were administered. On the preoperative CT at month 9, which showed stable disease compared with the CT at month 8, the primary mass measured 47 × 40 mm in the axial plane and 54 mm craniocaudally; no focal liver lesion was seen, and the adjacent lymph node measured 8 × 5 mm. The sum of target lesion diameters had therefore decreased from 136 mm to 47 mm (a 65% decrease), corresponding to a partial response, and the longest axial diameter of the primary mass alone had decreased from 123 mm to 47 mm (a 62% decrease).

Time point	Treatment or evaluation	Result
Diagnosis (Days 1-8)	CT and ultrasound-guided biopsy	Mass 12.3 × 11.0 × 11.8 cm; segment III lesion 13 × 11 mm; small round cell tumor, CD99+
After 3 cycles of VIDE	CT evaluation	Partial response (radiologist assessment); hepatic lesion regressed
After 6 cycles of VIDE	CT evaluation	Partial response (radiologist assessment); hepatic lesion further reduced; judged unresectable
After 2 cycles of VAI	CT evaluation	Stable disease
After 4 cycles of VAI (CT at months 8 and 9)	CT evaluation	Stable disease compared with the month 8 CT; primary mass 4.7 × 4.0 × 5.4 cm; no focal liver lesion; sum of target lesions 136 → 47 mm (-65%), partial response relative to baseline
Month 9	Surgical resection	6 × 4 × 3.5 cm specimen; >90% necrosis; margin <1 mm
Between surgery and radiotherapy	Postoperative consolidation chemotherapy	2 cycles of VAI
Four months after surgery	Adjuvant radiotherapy (VMAT)	45 Gy in 25 fractions (planned boost to 55.8 Gy omitted)

TABLE 1: Treatment timeline and tumor response.

Target lesions (RECIST 1.1): primary mass (123 mm) and segment III hepatic lesion (13 mm) at baseline; dimensions of the primary mass are given as axial × axial × craniocaudal.

VIDE: vincristine, ifosfamide, doxorubicin, etoposide; VAI: vincristine, actinomycin D, ifosfamide; VMAT: volumetric modulated arc therapy; CT: computed tomography; CD99: cluster of differentiation 99

The segment III hepatic lesion was considered suspicious for metastasis at diagnosis but was not biopsied. It had not been described on the referring CT performed four days earlier. It decreased in size on CT after three VIDE cycles, was not visualized on abdominal ultrasound after the fourth cycle, and had decreased further on CT after the sixth cycle. The preoperative CT at month 9 described no focal liver lesion and no new lesion, but a persistent opacification defect of the portal branch supplying segment III. This raises the possibility that the segment III abnormality reflected, at least in part, perfusion changes related to compression of the left portal branches by the tumor rather than a metastasis. At surgery, a cuff of liver segment III adherent to the tumor was resected, and this liver tissue showed no tumor on histological examination. However, the pathology report did not specifically identify the previously described lesion, and the lesion had already regressed on imaging before surgery, so its nature at diagnosis could not be established. The disease status at diagnosis, localized or metastatic, therefore remains indeterminate. CT images at diagnosis, before surgery, and after surgery at comparable anatomical levels are shown in Figure *3*.

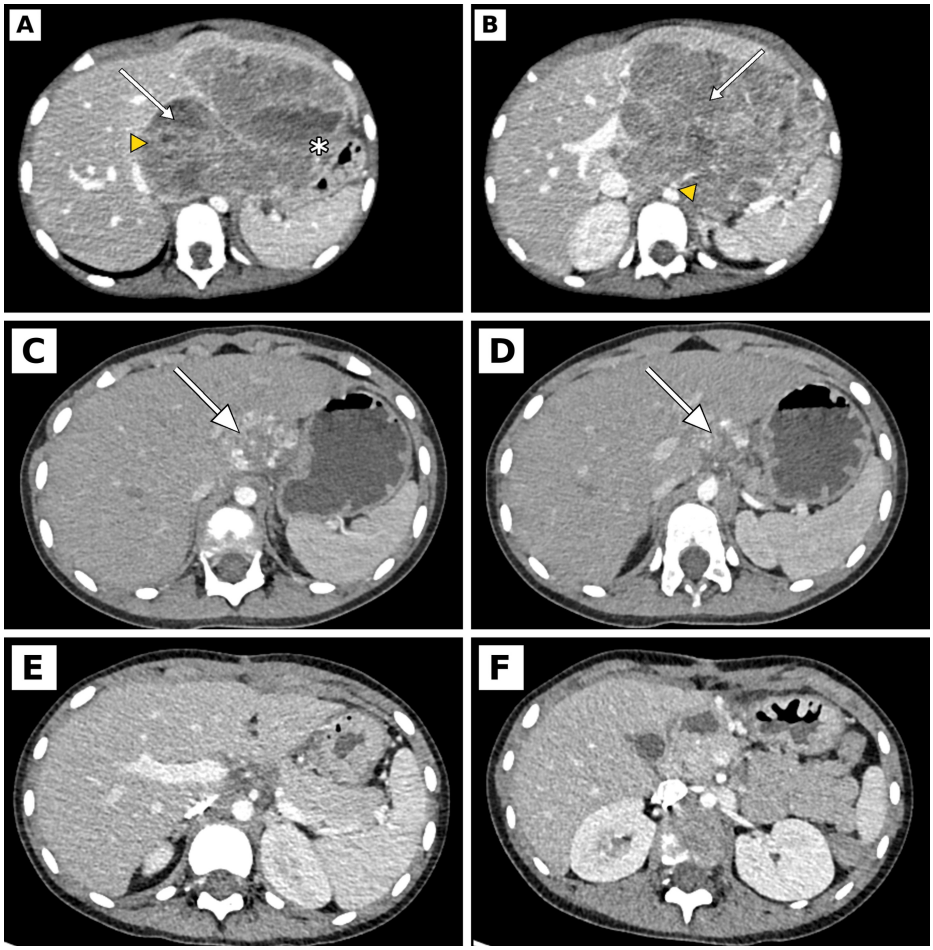


FIGURE 3: Axial contrast-enhanced CT of the upper abdomen at comparable levels at diagnosis (A, B; Day 5; same images as Figure 1), after induction chemotherapy before surgery (C, D; month 9), and after surgery (E, F; week 7).

(A, B) Large heterogeneous intraperitoneal mass measuring 12.3 × 11.0 cm in the axial plane (white arrows), in contact with the liver (yellow arrowhead in A), displacing the stomach (asterisk), and encasing the aorta (yellow arrowhead in B). (C, D) After 6 cycles of VIDE and 4 cycles of VAI, the residual mass (white arrows) is markedly smaller, measuring 4.7 × 4.0 cm in the axial plane, and contains calcifications and necrotic areas; the stomach is distended. (E, F) After resection, the mass is no longer visible at the corresponding levels; a hypodense area at the operative site, involving the lesser omentum and liver segment III (25 × 20 mm), was interpreted as postoperative change.

Nine months after diagnosis, the mass was resected through a supraumbilical midline laparotomy. It was firmly adherent to the diaphragm superiorly, the stomach, the posterior surface of liver segment III on the right, and the medial surface of the spleen on the left. Resection required dissection from both diaphragmatic crura, en bloc release from the stomach with ligation of the left gastric artery, and removal of a cuff of segment III that was intimately adherent to the tumor. The inferior part of the tumor was adherent to the left portal vein; a breach in the vein occurred during dissection and was repaired with sutures. The specimen measured 6 × 4 × 3.5 cm, which is consistent with the preoperative CT dimensions of the residual mass (4.7 × 4.0 cm in the axial plane and 5.4 cm craniocaudally), given that the specimen also included the resected liver cuff and surrounding tissue. It was lobulated and encapsulated, with alternating brown and white friable areas. It was entirely submitted for histological examination in 14 blocks. Microscopy showed residual CD99-positive small to medium-sized round cells with mitotic figures, surrounded by extensive treatment-related changes. These included necrosis, fibrosis, hemosiderin deposits, calcifications, cholesterol clefts, and a foreign-body giant cell reaction. The histological treatment response was estimated at more than 90% necrosis, which corresponds to a good response (less than 10% viable tumor; Salzer-Kuntschik grades I to III) [12]. The closest peripheral margin was less than 1 mm, and the surgical team classified the resection as microscopically incomplete (R1). The attached segment III liver tissue showed minimal chronic portal inflammation and no tumor. Postoperative CT of the chest, abdomen, and pelvis seven weeks after surgery showed a 25 × 20 mm hypodense area at the operative site, involving the lesser omentum and extending to liver segment III, which the radiologist interpreted as most likely related to the

hepatic resection. The left portal branch was no longer individualized. The rest of the liver was normal, and there was no lymphadenopathy, no pulmonary nodule, and no suspicious bone lesion (Figure *3*).

At the radiation oncology consultation in the month following surgery, the patient had a World Health Organization performance status of 1 and weighed 27 kg. Her abdominal scar was well healed, and no inguinal or supraclavicular lymph nodes were palpable. Postoperative consolidation chemotherapy resumed at that time in accordance with the Euro-Ewing protocol [10]. Because the resection was classified as R1, the multidisciplinary team recommended adjuvant radiotherapy. Simulation CT was performed approximately three months after surgery, with the patient supine on a positioning mattress. The plan was developed using the Monaco treatment planning system (Elekta AB, Stockholm, Sweden), and volumetric modulated arc therapy (VMAT) was delivered on a Versa HD linear accelerator (Elekta AB, Stockholm, Sweden). Patient positioning was checked with portal imaging.

The postoperative tumor bed, delineated as gross tumor volume 45 (GTV45), and its clinical target volume 45 (CTV45) were used to define the first planning target volume (PTV45), which was prescribed 45 Gy in 25 fractions of 1.8 Gy, five fractions per week. A sequential boost of 10.8 Gy in six fractions to planning target volume 55.8 (PTV55.8), derived from gross tumor volume 55.8 (GTV55.8) and encompassing the high-risk region, was initially planned for a total dose of 55.8 Gy (Figure *4*). CTV45 and clinical target volume 55.8 (CTV55.8) were defined using expansions of 1 cm and 1.5 cm from GTV45 and GTV55.8, respectively, adjusted for anatomical barriers. An institutional setup margin was then added to generate the planning target volumes. Dosimetry was performed in the same month, and several plans were compared. Organ-at-risk dose constraints could not be respected with the boost, so the multidisciplinary team decided to omit it to limit toxicity, and the total dose was limited to 45 Gy.

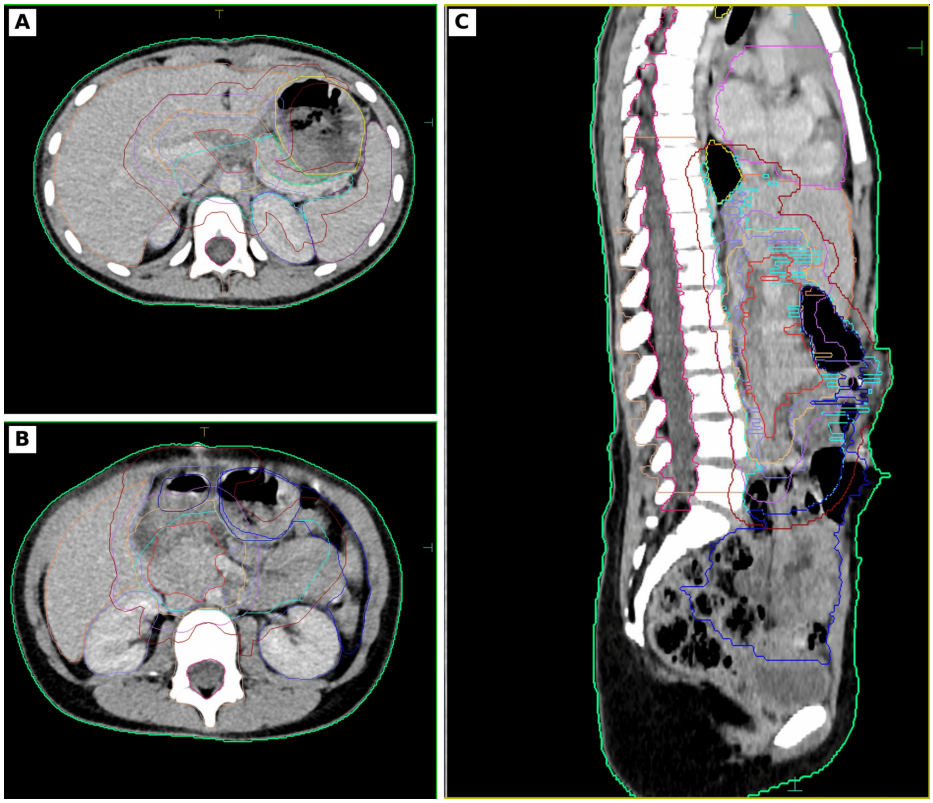


FIGURE 4: Radiotherapy target volumes and organs at risk on axial (A, B) and sagittal (C) planning computed tomography.

Target volumes: gross tumor volume 45 (GTV45, light purple), clinical target volume 45 (CTV45, cyan), planning target volume 45 (PTV45, dark red), gross tumor volume 55.8 (GTV55.8, red), clinical target volume 55.8 (CTV55.8, light orange), and planning target volume 55.8 (PTV55.8, violet). Organs at risk: liver (orange), stomach (yellow), duodenum (dark blue), small bowel (blue), pancreas (green), left kidney (blue-violet), right kidney (lavender), spleen (purple), spinal cord (pink), vertebrae (beige), and heart (magenta). The external body contour is shown in light green.

Target coverage and organ-at-risk doses of the delivered 45 Gy plan are shown in Table *2* and Figure *5*. The institutional planning objectives were informed largely by the Quantitative Analyses of Normal Tissue Effects in the Clinic (QUANTEC) recommendations [9]. All organ-at-risk objectives were met except for the pancreas, whose mean dose was 44.5 Gy, exceeding the 25 Gy objective because the gland lay within or

immediately adjacent to the target volumes. To respect the constraints of the bowel, stomach, and kidneys, PTV45 coverage was deliberately compromised: 74.6% of the PTV45 received at least 95% of the prescribed dose, whereas CTV45 coverage was maintained at 96.3%. The mean and maximum PTV45 doses were 42.8 Gy and 48.2 Gy, respectively. Radiotherapy started more than four months after surgery; this interval reflects the resumption of postoperative consolidation chemotherapy before radiotherapy, in accordance with the Euro-Ewing protocol. The overall treatment time was 61 days instead of the planned five weeks because of treatment interruptions related to the family's financial constraints. No chemotherapy was administered during radiotherapy. Acute toxicity, graded according to the Common Terminology Criteria for Adverse Events (CTCAE) version 5.0, was limited to grade 1 nausea, diarrhea, and epigastric pain. At the end of radiotherapy, she had a WHO performance status of 0 and no residual symptoms, and she was referred back to the pediatric oncology team. At the last follow-up, approximately three months after completion of radiotherapy and 18 months after diagnosis, she remained in good general condition under regular follow-up in the pediatric oncology department, with no clinical evidence of recurrence.

Structure	Planning objective	Achieved value
PTV45	V42.75Gy ≥ 95%	74.6% (not met)
PTV45	Dmean / Dmax (reported)	42.8 Gy / 48.2 Gy
CTV45	V42.75Gy ≥ 95%	96.3%
Small bowel	V45Gy ≤ 200 cm³	46.0 cm³
Small bowel	Dmean ≤ 30 Gy	19.4 Gy
Duodenum	V45Gy ≤ 33%	17.3%
Stomach	V45Gy ≤ 50 cm³	2.7 cm³
Stomach	Dmean ≤ 40 Gy	38.4 Gy
Left kidney	Dmean ≤ 18 Gy	16.6 Gy
Right kidney	Dmean ≤ 18 Gy	16.4 Gy
Liver	Dmean ≤ 30 Gy	23.6 Gy
Spleen	Dmean ≤ 40 Gy	34.8 Gy
Pancreas (whole gland)	Dmean ≤ 25 Gy	44.5 Gy (not met)
Pancreas (whole gland)	Dmin (reported)	33.7 Gy
Spinal cord	Dmax ≤ 45 Gy	34.6 Gy
Left lung	V20Gy ≤ 30%	24.8%
Right lung	V20Gy ≤ 30%	10.4%

TABLE 2: Target coverage and organ-at-risk doses of the delivered 45 Gy plan.

The pancreatic tail was not contoured separately.

V42.75Gy, V45Gy, V20Gy: volume receiving at least 42.75 Gy (95% of the prescribed dose), 45 Gy, or 20 Gy; Dmean: mean dose; Dmax: maximum dose; Dmin: minimum dose; PTV45: planning target volume 45; CTV45: clinical target volume 45; Gy: gray

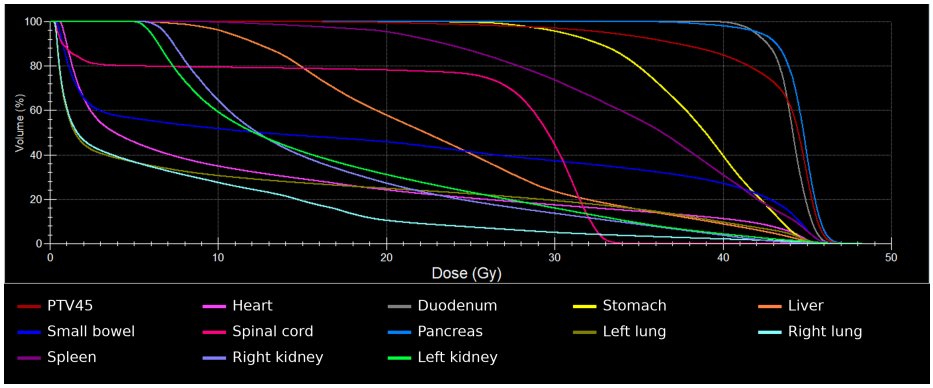


FIGURE 5: Dose-volume histogram of the delivered 45 Gy plan for target volumes and organs at risk.

Dose axis in gray. All organ-at-risk objectives were met except for the mean pancreatic dose; PTV45 coverage (V95%) was 74.6%, and CTV45 coverage was 96.3%.

PTV45: planning target volume 45; CTV45: clinical target volume 45; Gy: gray

Discussion

The main challenges in this case were the intra-abdominal location of the tumor, its encasement of the major vessels, and residual microscopic disease after chemotherapy and surgery. The diagnosis of probable EES was based on morphological and immunohistochemical findings, as t(11;22) and EWSR1 rearrangement testing was unavailable and was not performed.

EES accounted for 31% of Ewing sarcomas in one population-based study [3]. Compared with skeletal tumors, extraskeletal tumors were more likely to occur at axial sites and to affect older patients [3,5]. A pediatric meta-analysis of 29 studies identified the thorax and extremities as the most common sites [6]. Intestinal EES can present with non-specific symptoms and may mimic other gastrointestinal tumors on imaging, including gastrointestinal stromal tumor (GIST) [7]. Our patient presented with non-specific digestive symptoms and a large abdominal mass. Shankar and Konamme described an eight-year-old girl with abdominal wall EES who had a minimal histological response to six cycles of preoperative chemotherapy and underwent wide excision with negative margins [13]. In contrast, chemotherapy in our patient produced more than 90% necrosis, but the visceral location and vascular involvement made resection difficult, and margins were microscopically positive (R1). The prognostic significance of an extraskeletal origin remains unclear. A SEER study of 3,178 cases associated it with worse overall survival [4], whereas a Children's Oncology Group study of localized disease found better event-free survival for EES, with an adjusted hazard ratio of 0.69 [5]. Differences between the study populations should be considered when interpreting these results.

The differential diagnosis of an intraperitoneal small round cell tumor in a child includes DSRCT, neuroblastoma, rhabdomyosarcoma, lymphoblastic lymphoma, and sarcomas with capicua transcriptional repressor (CIC) or BCL6 corepressor (BCOR) alterations [2,8]. DSRCT is particularly relevant because it arises from abdominal serosal surfaces and also involves EWSR1. It typically expresses keratin and desmin, often with a dot-like pattern, and carries an EWSR1::Wilms tumor 1 (WT1) fusion associated with t(11;22)(p13;q12) [8]. In this patient, diffuse membranous CD99 staining, together with negative desmin, myogenin, CD45, and neuroendocrine markers, was suggestive of Ewing sarcoma. However, CD99 is not specific [2]. European guidelines recommend molecular confirmation of an EWSR1 or FUS rearrangement with an ETS partner [1]. Testing for t(11;22) and EWSR1 rearrangement was unavailable at our hospital and was not performed, so the diagnosis remains probable EES pending molecular confirmation, and DSRCT could not be excluded. The response to treatment was compatible with Ewing sarcoma but could not confirm the molecular diagnosis. Negative desmin staining argues against DSRCT without excluding it, as desmin was expressed in 90% of cases in the series by Gerald et al. [8]. Additional immunostains could have strengthened the assessment, including NK2 homeobox 2 (NKX2.2), a sensitive marker for Ewing sarcoma [14], and WT1 directed against the C-terminus, which can help distinguish DSRCT from Ewing sarcoma [15].

The patient received VIDE induction, the European standard before the EURO EWING 2012 trial [10,16]. That trial showed better event-free survival and a more favorable toxicity profile with interval-compressed VDC/IE (vincristine, doxorubicin, and cyclophosphamide alternating with ifosfamide and etoposide), supporting its use as a preferred frontline regimen [16]. VAI was the comparator consolidation regimen in Euro-EWING99, which evaluated cyclophosphamide-based VAC (vincristine, actinomycin D, and cyclophosphamide) against VAI in standard-risk localized disease [10]. Histological response is

prognostically relevant [17,18], and the response exceeding 90% in this patient was consistent with a good response. The Euro-E.W.I.N.G.99 and Ewing-2008 trials showed improved outcomes with busulfan-melphalan consolidation and autologous stem-cell rescue in selected patients with localized high-risk disease, including poor histological responders [17]. This approach was not used in our patient. Instead, additional preoperative VAI cycles were given in an attempt to make the mass resectable, and stable findings on serial CT supported the decision to proceed with surgery.

Surgery is preferred when complete resection is feasible without unacceptable morbidity. Radiotherapy is recommended for unresectable disease or after an inadequate resection [1]. Margin status and histological response help guide the decision to use postoperative radiotherapy [1,19]. In an analysis of 1,058 patients treated in the Cooperative Ewing's Sarcoma Study (CESS) 81 and CESS 86 and the European Intergroup Cooperative Ewing's Sarcoma Study (EICESS) 92 trials, postoperative radiotherapy improved local control after intralesional resection and after wide resection in patients with a poor histological response [19]. A multistate analysis of 982 patients also associated marginal or intralesional resection and pelvic or axial location with local recurrence, while radiotherapy was associated with a lower risk [18]. Our patient had more than 90% necrosis but an R1 resection at an axial visceral site. The multidisciplinary team therefore recommended adjuvant radiotherapy, in keeping with its role after inadequate resection [1,19].

Abdominal radiotherapy is challenging because the bowel, kidneys, liver, and spinal cord lie close to the target. QUANTEC provides a framework for assessing dose-volume effects, but the general review does not validate every objective in Table *2* as a pediatric tolerance [9]. These values should therefore be understood as the planning objectives used for this patient. With VMAT, the mean kidney doses were below 17 Gy, the mean liver dose was 23.6 Gy, and the maximum spinal cord dose was 34.6 Gy. These results were obtained at the cost of reduced PTV45 coverage (V95% of 74.6%), although CTV45 coverage remained adequate (V95% of 96.3%); underdosage at the PTV margin may further increase the risk of marginal recurrence. The planned boost to 55.8 Gy could not be delivered within the organ-at-risk constraints, and the total dose was limited to 45 Gy. Several considerations supported this decision. First, 45 Gy was the median postoperative dose in the CESS 86 and EICESS 92 trials, in which postoperative radiotherapy achieved high local control rates [19,20]. Second, the histological response was good, with more than 90% necrosis, a factor associated with a lower risk of local failure [18,19]. Third, the boost volume lay against the duodenum, stomach, and small bowel, and escalation to 55.8 Gy would have exceeded their planning objectives in a young child. Nevertheless, 45 Gy lies at the lower end of postoperative doses used for microscopic residual disease, and a higher risk of local recurrence cannot be excluded, which justifies close surveillance of the tumor bed. Radiotherapy started more than four months after surgery because postoperative consolidation chemotherapy was resumed first, as planned in the Euro-Ewing protocol [10]. Systemic treatment therefore continued during this interval. In the CESS 86 and EICESS 92 trials, five-year local control was 98% when postoperative radiotherapy began within 60 days and 92% when it began later, a difference that was not statistically significant [20]. In addition, the overall treatment time was prolonged by about four weeks because of interruptions related to the family's financial constraints, which may have reduced the biological effectiveness of the delivered dose and added to the uncertainty about local control. This illustrates the compromise often required between local control and toxicity in pediatric abdominal irradiation. Pancreatic sparing was particularly difficult, with a mean dose of 44.5 Gy to the whole pancreas. The pancreatic tail was not contoured separately, but the minimum dose to the whole gland was 33.7 Gy, so the tail necessarily received more than 30 Gy. In a cohort of childhood cancer survivors, the risk of diabetes increased with radiation dose to the pancreatic tail up to 20-29 Gy and then plateaued [21]. As this exceeds the dose range at which the risk plateaued, this patient should therefore be considered at increased risk of diabetes mellitus, and high pancreatic doses may also impair exocrine function. Long-term follow-up should include periodic screening for diabetes, attention to symptoms of malabsorption, and monitoring of renal function, growth, and cardiac effects related to anthracycline therapy [22].

The main limitation is the lack of molecular confirmation. Testing for t(11;22) and EWSR1 rearrangement was unavailable at our hospital and was not performed. The diagnosis therefore remains probable EES pending molecular confirmation: the morphology and immunohistochemistry were suggestive of Ewing sarcoma, but DSRCT and other undifferentiated round cell sarcomas were not excluded [1,2,8]. The hepatic lesion was not biopsied before treatment, and although the resected segment III tissue was tumor-free, it was obtained after the lesion had regressed; the disease status at diagnosis is therefore reported as indeterminate rather than inferred. PET-CT was not performed, and baseline vital signs and laboratory values could not be retrieved. Follow-up after radiotherapy is still short, and local control and late treatment effects cannot yet be assessed.

Conclusions

This case describes the management of an intraperitoneal small round cell tumor in a young child, diagnosed as probable EES on morphological and immunohistochemical grounds, pending molecular confirmation, with DSRCT not excluded. Prolonged induction chemotherapy allowed resection of a tumor that was initially unresectable because of major vascular encasement, with more than 90% treatment-related necrosis but microscopically positive margins. Adjuvant radiotherapy was limited to 45 Gy to respect organ-at-risk constraints, at the cost of a high pancreatic dose. The diagnosis remains uncertain, the disease status at diagnosis is indeterminate, and follow-up after radiotherapy is short, so no conclusion can be drawn

about long-term local control or late effects. This case highlights the importance of access to molecular testing and the need for prolonged surveillance of local control and late toxicity.

Additional Information

Author Contributions

All authors have reviewed the final version to be published and agreed to be accountable for all aspects of the work.

Concept and design: Fatima Benhjar, Soumiya Samba, Mohamed Moukhlissi, Soufiane Berhili, Ahmed BenSghier, Loubna Mezouar

Acquisition, analysis, or interpretation of data: Fatima Benhjar, Soumiya Samba, Mohamed Moukhlissi, Soufiane Berhili, Ahmed BenSghier, Loubna Mezouar

Drafting of the manuscript: Fatima Benhjar, Soumiya Samba, Mohamed Moukhlissi, Soufiane Berhili, Ahmed BenSghier, Loubna Mezouar

Critical review of the manuscript for important intellectual content: Fatima Benhjar, Soumiya Samba, Mohamed Moukhlissi, Soufiane Berhili, Ahmed BenSghier, Loubna Mezouar

Supervision: Mohamed Moukhlissi, Soufiane Berhili, Ahmed BenSghier, Loubna Mezouar

Disclosures

Human subjects: Informed consent for treatment and open access publication was obtained or waived by all participants in this study. **Conflicts of interest:** In compliance with the ICMJE uniform disclosure form, all authors declare the following: **Payment/services info:** All authors have declared that no financial support was received from any organization for the submitted work. **Financial relationships:** All authors have declared that they have no financial relationships at present or within the previous three years with any organizations that might have an interest in the submitted work. **Other relationships:** All authors have declared that there are no other relationships or activities that could appear to have influenced the submitted work.

References

1. Strauss SJ, Frezza AM, Abecassis N, et al.: Bone sarcomas: ESMO-EURACAN-GENTURIS-ERN PaedCan clinical practice guideline for diagnosis, treatment and follow-up. Ann Oncol. 2021, 32:1520-36. 10.1016/j.annonc.2021.08.1995
2. Dehner CA, Lazar AJ, Chrisinger JS: Updates on WHO classification for small round cell tumors: Ewing sarcoma vs. everything else. Hum Pathol. 2024, 147:101-13. 10.1016/j.humpath.2024.01.007
3. Applebaum MA, Worch J, Matthay KK, Goldsby R, Neuhaus J, West DC, Dubois SG: Clinical features and outcomes in patients with extraskeletal Ewing sarcoma. Cancer. 2011, 117:3027-32. 10.1002/cncr.25840
4. Jiang S, Wang G, Chen J, Dong Y: Comparison of clinical features and outcomes in patients with extraskeletal vs skeletal Ewing sarcoma: an SEER database analysis of 3,178 cases. Cancer Manag Res. 2018, 10:6227-36. 10.2147/CMAR.S178979
5. Cash T, McIlvaine E, Krailo MD, et al.: Comparison of clinical features and outcomes in patients with extraskeletal versus skeletal localized Ewing sarcoma: a report from the Children's Oncology Group. Pediatr Blood Cancer. 2016, 63:1771-9. 10.1002/pbc.26096
6. Ghandour M, Lehner B, Klotz M, Geisbüsch A, Bollmann J, Renkawitz T, Horsch A: Extraosseous Ewing sarcoma in children: a systematic review and meta-analysis of clinicodemographic characteristics. Children (Basel). 2022, 9:1859. 10.3390/children9121859
7. Luo B, Gao W, Li T, Yu X, Guo F: Primary Ewing's sarcoma of the intestine: case report and literature review . Front Oncol. 2024, 14:1357945. 10.3389/fonc.2024.1357945
8. Gerald WL, Ladanyi M, de Alava E, Cuatrecasas M, Kushner BH, LaQuaglia MP, Rosai J: Clinical, pathologic, and molecular spectrum of tumors associated with t(11;22)(p13;q12): desmoplastic small round-cell tumor and its variants. J Clin Oncol. 1998, 16:3028-36. 10.1200/JCO.1998.16.9.3028
9. Marks LB, Yorke ED, Jackson A, et al.: Use of normal tissue complication probability models in the clinic . Int J Radiat Oncol Biol Phys. 2010, 76:S10-9. 10.1016/j.ijrobp.2009.07.1754
10. Le Deley MC, Paulussen M, Lewis I, et al.: Cyclophosphamide compared with ifosfamide in consolidation treatment of standard-risk Ewing sarcoma: results of the randomized noninferiority Euro-EWING99-R1 trial. J Clin Oncol. 2014, 32:2440-8. 10.1200/JCO.2013.54.4833
11. Eisenhauer EA, Therasse P, Bogaerts J, et al.: New response evaluation criteria in solid tumours: revised RECIST guideline (version 1.1). Eur J Cancer. 2009, 45:228-47. 10.1016/j.ejca.2008.10.026
12. Salzer-Kuntschik M, Delling G, Beron G, Sigmund R: Morphological grades of regression in osteosarcoma after polychemotherapy - study COSS 80. J Cancer Res Clin Oncol. 1983, 106:21-4. 10.1007/BF00625047
13. Shankar G, Konamme VK: Abdominal wall extraskeletal Ewing's sarcoma in an 8-year-old child . J Indian Assoc Pediatr Surg. 2022, 27:771-4. 10.4103/jiaps.jiaps_46_22
14. Yoshida A, Sekine S, Tsuta K, Fukayama M, Furuta K, Tsuda H: NKX2.2 is a useful immunohistochemical marker for Ewing sarcoma. Am J Surg Pathol. 2012, 36:993-9. 10.1097/PAS.0b013e31824ee43c

15. Hill DA, Pfeifer JD, Marley EF, Dehner LP, Humphrey PA, Zhu X, Swanson PE: WT1 staining reliably differentiates desmoplastic small round cell tumor from Ewing sarcoma/primitive neuroectodermal tumor: an immunohistochemical and molecular diagnostic study. Am J Clin Pathol. 2000, 114:345-53. 10.1093/ajcp/114.3.345
16. Brennan B, Kirton L, Marec-Bérard P, et al.: Comparison of two chemotherapy regimens in patients with newly diagnosed Ewing sarcoma (EE2012): an open-label, randomised, phase 3 trial. Lancet. 2022, 400:1513-21. 10.1016/S0140-6736(22)01790-1
17. Whelan J, Le Deley MC, Dirksen U, et al.: High-dose chemotherapy and blood autologous stem-cell rescue compared with standard chemotherapy in localized high-risk Ewing sarcoma: results of Euro-E.W.I.N.G.99 and Ewing-2008. J Clin Oncol. 2018, 36:3110-9. 10.1200/JCO.2018.78.2516
18. Bosma SE, Rueten-Budde AJ, Lancia C, et al.: Individual risk evaluation for local recurrence and distant metastasis in Ewing sarcoma: a multistate model for Ewing sarcoma. Pediatr Blood Cancer. 2019, 66:e27943. 10.1002/pbc.27943
19. Schuck A, Ahrens S, Paulussen M, et al.: Local therapy in localized Ewing tumors: results of 1058 patients treated in the CESS 81, CESS 86, and EICESS 92 trials. Int J Radiat Oncol Biol Phys. 2003, 55:168-77. 10.1016/S0360-3016(02)03797-5
20. Schuck A, Rübe C, Könemann S, et al.: Postoperative radiotherapy in the treatment of Ewing tumors: influence of the interval between surgery and radiotherapy. Strahlenther Onkol. 2002, 178:25-31. 10.1007/s00066-002-0883-1
21. de Vathaire F, El-Fayech C, Ben Ayed FF, et al.: Radiation dose to the pancreas and risk of diabetes mellitus in childhood cancer survivors: a retrospective cohort study. Lancet Oncol. 2012, 13:1002-10. 10.1016/S1470-2045(12)70323-6
22. DeVine A, Landier W, Hudson MM, et al.: The Children's Oncology Group long-term follow-up guidelines for survivors of childhood, adolescent, and young adult cancers: a review. JAMA Oncol. 2025, 11:544-53. 10.1001/jamaoncol.2024.6812